Experimental realization of Hamiltonian tomography by quantum quenches

Xi Chen,[1,2] Yuchen Li,[1,2] Ze Wu,[1,2] Ran Liu ⬤,[1,2] Zhaokai Li,[1,2,3] and Hui Zhou ⬤[4,5,*]

[1]*Hefei National Laboratory for Physical Sciences at the Microscale and Department of Modern Physics,*
University of Science and Technology of China, Hefei 230026, China
[2]*CAS Key Laboratory of Microscale Magnetic Resonance, University of Science and Technology of China, Hefei 230026, China*
[3]*Synergetic Innovation Center of Quantum Information and Quantum Physics,*
University of Science and Technology of China, Hefei 230026, China
[4]*Department of Physics, Shaanxi University of Science and Technology, Xi'an, 710021 Shaanxi, China*
[5]*Institute of Theoretical Physics, Shaanxi University of Science and Technology, Xi'an, 710021 Shaanxi, China*

The parameter estimation of the Hamiltonian of an unknown quantum system is essential in quantum information processing. However, the general methods based on quantum state tomography and process tomography are resource demanding and challenging in large quantum systems. On the other hand, if the interaction form of a system is known, one can adopt the quantum quench protocol to reconstruct the generic many-body Hamiltonian with local interactions, requiring significantly lower complexity and measurement cost compared to the general tomography technique. Here we report an experimental demonstration of the quench method to determine the scalar coupling constants in a three-spin chain. In the experiments, we demonstrate that how the quality of the estimation is affected by the duration of the quench and the number of input states. Our results show that the quantum quench protocol is a promising strategy to implement Hamiltonian estimation for many-body systems, especially when the cost of measurement is crucial in practical cases.

I. INTRODUCTION

The ability to efficiently achieve the full knowledge of quantum many-body Hamiltonians is a nontrivial problem in quantum physics and quantum information science [1–4]. As a universal approach to characterize the unknown quantum states and dynamics, quantum tomography [5–7] has been widely used on different physical systems, such as nuclear magnetic resonance (NMR) [8], nitrogen-vacancy centers in diamond [9–11], photonics [12,13], ion traps [14,15], and superconducting circuits [16]. However, it is intractable to perform a complete state or process tomography in large-scale quantum many-body systems, due to the exponentially growing resources required, including the number of experiments and computational time of postprocessing. Therefore, most of the implementations are limited to small and special many-body systems [8–21].

To overcome this obstacle, substantial schemes have been proposed to reduce the complexity and resources in identifying a system Hamiltonian, including via compressive sensing and the machine-learning method [22–24], time-dependent measurement records [25–31], and the Zeeman effect avoiding the measurement on time-dependent quantities [32]. Here we focus on the quantum quench protocol which can reconstruct the generic local many-body Hamiltonian with only local measurements on the initial and final evolving states governed by the system Hamiltonian [33]. The basic ideal is to solve a system of polynomial equations, derived from the generalized energy conservation at any time, with respect to the unknown parameters in the Hamiltonian. By means of many pairs of initial and final states with a fixed quench duration, it is immune to the complexity in experiment and computation, and the Hamiltonian can be determined uniquely. An experiment is needed to bridge the gap between the theoretical proposal and practical application.

In this work we report an experimental implementation of this scheme to measure the scalar couplings of a three-spin quantum system polarized in an NMR setup. Compared with the results obtained through a Fourier transform on temporal records of the system observables [34,35], our experiment presents a fairly good estimation with many fewer experimental measurements performed and shorter dynamical evolution.

The rest of this paper is organized as follows. In Sec. II we review the theoretical background of Hamiltonian tomography via the quantum quench method [33]. Section III describes the experimental details of estimating the spin-spin interaction strengths in a three-spin heteronuclear system by taking the transverse radio-frequency (rf) field as the standard of calibration. Then we provide an error analysis of the measurement, decoherence, and off-resonance effect. Finally, a brief summary with a discussion is presented in Sec. IV.

II. THEORETICAL BACKGROUND

Here we briefly review the quantum quench scheme in Ref. [33]. Consider a quantum many-body system with the time-independent Hamiltonian

$$H = \sum_{\alpha=1}^{n} c_\alpha O_\alpha, \tag{1}$$

*zhouhui9240@163.com

where O_α is the Hermitian matrix, c_α is the unknown parameter to be estimated, and n is the number of these unknown parameters. Here n is assumed to scale polynomially with the system size, which usually holds for realistic physical systems. Given the initial state $|\psi(0)\rangle$, the system governed by Eq. (1) can be described as $|\psi(T)\rangle = e^{-iHT}|\psi(0)\rangle$ at time T, which satisfies

$$\langle\psi(t)|H^m|\psi(t)\rangle = \langle\psi(0)|H^m|\Psi(0)\rangle \,\forall\, m \in \mathbb{N}. \quad (2)$$

Substituting Eq. (1) into Eq. (2) with $m = 1, 2, 3, \ldots$ yields a system of polynomial equations in relation to the unknown parameters $\{c_\alpha\}$. In principle, these parameters can be uniquely derived using any pair of states $|\psi(0)\rangle$ and $|\psi(T)\rangle$ with $m = 1, 2, 3, \ldots, n$ as long as the number of unknown parameters $n \leqslant D - 1$, where D is the system dimension.

However, the complexity in experiment and computation, resulting from the higher-order ($m \geqslant 2$) equations in Eq. (2), will make it difficult to implement this scheme in practice. Here we adopt the multiple quenches protocol [33] by using $m = 1$ in Eq. (2) only and p pairs of initial and final states,

$$\{|\psi_i(0)\rangle \rightarrow |\psi_i(T)\rangle = e^{-iHT}|\psi_i(0)\rangle, \ i = 1, 2, \ldots, p\}. \quad (3)$$

Then we can obtain a linear system of equations $\mathbb{M}\vec{c} = 0$, where the column vector $\vec{c} = [c_1, c_2, c_3, \ldots, c_n]^T$ and $\mathbb{M}$ represents a $p \times n$ matrix with the element in the ith row and the αth column

$$\mathbb{M}_{i\alpha} = \langle\psi_i(0)|O_\alpha|\psi_i(0)\rangle - \langle\psi_i(T)|O_\alpha|\psi_i(T)\rangle. \quad (4)$$

Note that these expectations could be measured in experiment. To avoid confusion, $\mathbb{M}$ only denotes the theoretical matrix above, and the symbol M is used to stand for the experimental matrix throughout the text. Then we will have a linear homogeneous system of equations $M\vec{x} = 0$ with the symbol $\vec{c}$ replaced by the undetermined $\vec{x}$. If the rank of M is $n - 1$, the solution of $M\vec{x} = 0$ will be $\vec{c}$ up to a multiplier scale. Hence, we can use at least $n - 1$ equations to exactly acquire the parameters $\{c_\alpha\}$ up to an overall multiplicative factor. In experiment the noises will inevitably lead to the imperfection of M and thus the deviations of unknown parameters; we can use more than $n - 1$ pairs of initial and final states to mitigate these deviations. In this case, the best estimation of the solution of $M\vec{x} = 0$ is obtained from the least-squares method, which is the right singular vector of M with the smallest singular value (or, equivalently, the eigenvector of $M^T M$ with the smallest eigenvalue) [33,36].

A summary of the general procedure for Hamiltonian tomography is as follows.

(a) Prepare the initial state $|\psi_i(0)\rangle$ randomly and measure the expectations $\langle O_\alpha(0)\rangle = \langle\psi_i(0)|O_\alpha|\psi_i(0)\rangle$, $\alpha = 1, 2, \ldots, n$. Note that if $|\psi_i(0)\rangle$ is the eigenstate of the system Hamiltonian, this system will remain unchanged during evolution except for a global phase; thus we cannot reconstruct the Hamiltonian because the matrix M is just equal to zero.

(b) Steer the system under the Hamiltonian H for a fixed quench time T towards the final state $|\psi_i(T)\rangle$ and measure the expectations $\langle O_\alpha(T)\rangle = \langle\psi_i(T)|O_\alpha|\psi_i(T)\rangle$ with $\alpha = 1, 2, \ldots, n$.

(c) Obtain the M matrix according to Eq. (4) and solve the linear system of equations $M\vec{x} = 0$ via the least-squares method.
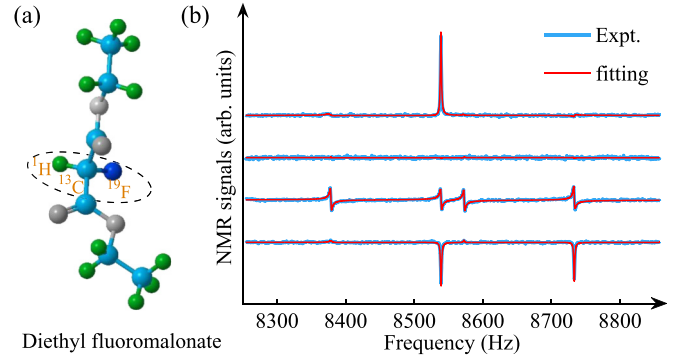

FIG. 1. (a) Molecule structure for diethyl fluoromalonate. (b) ^{13}C experimental spectra (blue thick lines) and fitting spectra (red thin lines). The top line is the spectrum of state $|000\rangle$ after a $\pi/2$ pulse applied on the carbon channel. The other three lines denote the spectra of the state $\frac{1}{\sqrt{2}}(|0\rangle - |1\rangle) \otimes |0\rangle \otimes \frac{1}{\sqrt{2}}(i|0\rangle + |1\rangle)$ by applying $\pi/2$ readout pulses along the x axis on ^{13}C, ^{1}H, and ^{19}F, respectively.

From the above procedure it can be seen that the number of measurements required is proportional to the number of elements in the matrix M, i.e., $O(n^2)$, which provides promising Hamiltonian tomography technology for the quantum systems suffering from expensive and time-consuming measurements. In addition, the computing cost of the postprocessing, i.e., the singular value decomposition, is also polynomial with the size of the matrix M [36].

III. EXPERIMENT

The experiment is conducted on a Bruker Advance III 400-MHz spectrometer at room temperature. The quantum system we study is the diethyl fluoromalonate molecule dissolved in deuterated chloroform, whose structure is shown in Fig. 1(a), with the ^{13}C, ^{1}H, and ^{19}F spins being labeled as qubits 1, 2, and 3, respectively. By setting the oscillating frequencies of three transverse rf fields as the corresponding resonant frequencies of the three spins, the Hamiltonian of this quantum system in the rotating frame [37] is

$$H_{\text{int}} = \sum_{1 \leqslant j < k}^{3} \frac{\pi}{2} J_{jk} \sigma_z^j \sigma_z^k, \quad (5)$$

where σ_ν^j denotes the Pauli matrix of jth spin with $\nu = x, y, z$, and J_{jk} is the to-be-estimated scalar coupling constant between spin j and k. In the whole experiment, we apply assistant transverse rf fields to the three spins, which not only can break the commutability in Eq. (5) to encode information of the Hamiltonian to the M matrix, but also can be used as a reference to determine the multiplicative factor. As a result, the Hamiltonian of this physical system reads

$$H_{\text{phys}} = \pi \sum_{k=1}^{3} \omega_{\text{rf}}^k \sigma_x^k + \sum_{1 \leqslant j < k}^{3} \frac{\pi}{2} J_{jk} \sigma_z^j \sigma_z^k, \quad (6)$$

where ω_{rf}^k is the rotation frequency (in hertz) of the kth qubit driven by the rf field. Comparing Eq. (6) with Eq. (1), we
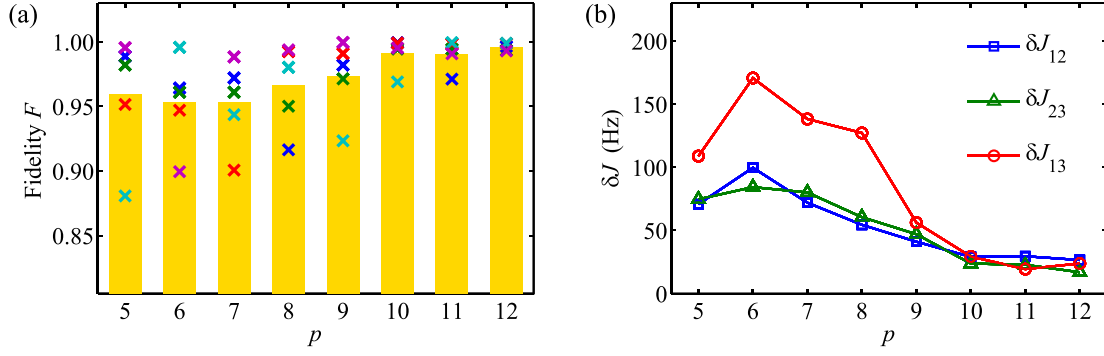
FIG. 2. (a) Experimental fidelities F and (b) mean absolute error δJ versus the number of quantum quenches p in five repeated experiments. The colored crosses and yellow bars in (a) represent the fidelities and average values at every p, respectively. The different symbols in (b) represent the mean absolute errors of couplings J_{12}, J_{23}, and J_{13} according to Eq. (10). Here the duration of quantum quench is set equal to $T = 10$ ms.

now have a target Hamiltonian with $\{O_\alpha \ (\alpha = 1, 2, \ldots, 6)\} = \{\sigma_x^1, \sigma_x^2, \sigma_x^3, \sigma_z^1\sigma_z^2, \sigma_z^2\sigma_z^3, \sigma_z^1\sigma_z^3\}$ and the relations

$$c_1 = \pi\omega_{\mathrm{rf}}^1, \quad c_2 = \pi\omega_{\mathrm{rf}}^2, \quad c_3 = \pi\omega_{\mathrm{rf}}^3,$$
$$c_4 = \frac{\pi}{2}J_{12}, \quad c_5 = \frac{\pi}{2}J_{23}, \quad c_6 = \frac{\pi}{2}J_{13}. \tag{7}$$

Then we will experimentally estimate the scalar couplings of this liquid sample with the help of the aforementioned method.

A. Experimental procedures and results

For the ith ($i = 1, 2, 3, \ldots, p$) quench, the quantum system is first initialized to

$$|\psi_i(0)\rangle = |\phi_1\rangle \otimes |\phi_2\rangle \otimes |\phi_3\rangle. \tag{8}$$

Here $|\phi_j\rangle$ ($j = 1, 2, 3$) can be randomly chosen from the pool $\mathbb{A} = \{\frac{1}{\sqrt{2}}(|0\rangle \pm |1\rangle), \frac{1}{\sqrt{2}}(i|0\rangle \pm |1\rangle), |0\rangle, |1\rangle\}$, which consists of the eigenstates of σ_ν ($\nu = x, y, z$). These types of initial states are sufficiently distinct from each other [33,38] and can provide independent information about the Hamiltonian (6). From the (pseudo)pure state $|000\rangle$ prepared in experiment [39,40], the initial state $|\psi_i(0)\rangle$ can be created easily through random local operations on three qubits from the set $\mathbb{U} = \{R_x(\frac{\pi}{2}), R_x(-\frac{\pi}{2}), R_y(\frac{\pi}{2}), R_y(-\frac{\pi}{2}), R_y(\pi), I_2\}$. Here $R_\nu(\theta)$ represents θ-rotation pulse along the ν axis and I_2 represents the 2×2 identity operator. Then, driven under the Hamiltonian H_{phys} for a fixed duration T, the final state becomes $|\psi_i(T)\rangle = e^{-iH_{\mathrm{phys}}T} |\psi_i(0)\rangle$. Note that the auxiliary transverse rf fields are applied on the three spins during the whole quantum quench.

To obtain the elements in the M matrix, we use readout operations $R_x^j(\frac{\pi}{2})$ ($j = 1, 2, 3$) to measure the expectations of local operators $\{O_\alpha\}$ for the initial state $|\psi_i(0)\rangle$ and final state $|\psi_i(T)\rangle$. In our experiment, all the signals of ^{1}H and ^{19}F are transferred to ^{13}C and then read out from the ^{13}C spectra [41]. For example, the experimental readout spectra for the first initial state $|\psi_1(0)\rangle = \frac{1}{\sqrt{2}}(|0\rangle - |1\rangle) \otimes |0\rangle \otimes \frac{1}{\sqrt{2}}(i|0\rangle + |1\rangle)$ are displayed in Fig. 1(b). The expectation $\langle O_\alpha \rangle$ can be obtained from the peak intensities by fitting the spectra to a sum of four Lorentz functions: The sum of all four real intensities of the peaks gives the expectation $\langle \sigma_x^j \rangle$, and the expectation

$\langle \sigma_z^j \sigma_z^k \rangle$ ($k \neq j$) is obtained from a linear combination of the four imaginary intensities [35].

According to the above process, we can obtain the $p \times 6$ matrix M by quenching the quantum system p times and get a general solution by solving $M\vec{x} = 0$ up to an overall multiplicative factor. Then, combined with Eq. (7), the scalar couplings can be acquired directly from the last three numbers in the solution. To analyze the performance of this tomography proposal, we utilize the exact values of scalar couplings by traditional method [34,35] as reference, i.e., $\mathbb{J}_{12} = 160.6 \pm 2.1$ Hz, $\mathbb{J}_{23} = 48.0 \pm 1.9$ Hz, and $\mathbb{J}_{13} = -194.4 \pm 2.1$ Hz. These values are obtained from the Fourier transform on about 4×10^3 expectations measured over an approximately 3×10^3 ms sampling duration (free-induction decay signals). Here we define the fidelity between exact parameters $\vec{J}_{\mathrm{th}}$ and reconstructed parameters $\vec{J}_{\mathrm{expt}}$ in experiments as

$$F = \left| \frac{\vec{J}_{\mathrm{th}} \cdot \vec{J}_{\mathrm{expt}}}{\|\vec{J}_{\mathrm{th}}\| \cdot \|\vec{J}_{\mathrm{expt}}\|} \right|, \tag{9}$$

where $\vec{J}_{\mathrm{th}} = [\mathbb{J}_{12}, \mathbb{J}_{23}, \mathbb{J}_{13}]$, $\vec{J}_{\mathrm{expt}} = [J_{12}, J_{23}, J_{13}]$, and $\| \cdot \|$ represents the Euclidean norm. Equation (9) describes the angle between vectors $\vec{J}_{\mathrm{expt}}$ and $\vec{J}_{\mathrm{th}}$ and is independent of the multiplicative factor.

In order to investigate the influence of the number of quenches p on the final results in experiments, we fix the time interval $T = 10$ ms and measure the reconstructed parameters $\vec{J}_{\mathrm{expt}}$ for different p. As shown in Fig. 2(a), the mean fidelity (yellow bar) of five repeated experiments (crosses) goes up gradually as p increases: $\overline{F}$ is 0.960 for $p = 5$, while it reaches 0.996 for $p = 12$. Moreover, the corresponding standard deviation decreases from 0.047 to 0.003. To further acquire the absolute scalar constants, we take the value of the transverse field $\omega_{\mathrm{rf}}^1 = 100$ Hz applied in experiment as reference. When the number of quantum quenches $p = 12$, the couplings reconstructed in experiment are $J_{12} = 175.3$ Hz, $J_{23} = 39.3$ Hz, and $J_{13} = -198.0$ Hz with the average deviation $\overline{\delta J} = \frac{1}{3}\sum_{1 \leqslant j < k}^3 |J_{ij} - \mathbb{J}_{ij}| \approx 9$ Hz. Figure 2(b) shows that the mean absolute error (MAE) δJ_{ij} of the three couplings in these five repeated experiments decreases in general with the increment of the number of quantum quenches p. Here the
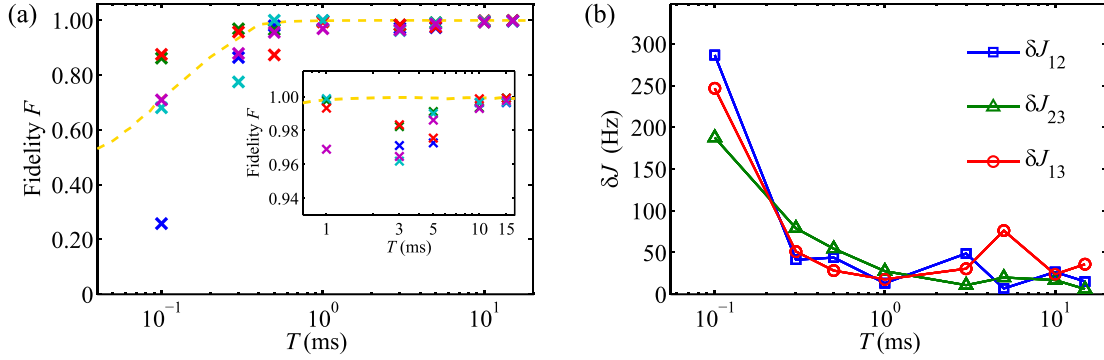
FIG. 3. (a) Experimental fidelities F and (b) mean absolute errors δJ versus quench duration T in five experiments. The number of quantum quenches p is 12. In (a) the colored crosses represent the fidelities in five experiments. The dashed line represents the numerical simulation results by adding random normal distribution errors (with standard deviation 0.04) to the ideal matrix $\mathbb{M}$. Here each point in this line is averaged over 2×10^4 results. In (b) the different symbols display the mean absolute errors of the three couplings measured in five experiments.

MAE δJ_{ij} is defined by

$$\delta J_{ij} = \frac{1}{L} \sum_{l=1}^{L} \left| J_{ij}^l - \mathbb{J}_{ij} \right|, \qquad (10)$$

with the lth experimental result J_{ij}^l and repeated $L = 5$ times. Therefore, more pairs of initial and final states will make the reconstructed results more robust against the noises in practice.

We also explore how the time interval T influences the performance of this proposal in experiment by setting quench times $p = 12$ and changing the duration T. In five repeated experiments, as shown in Fig. 3(a), the experimental fidelities (crosses) have a considerable dispersion over a short duration T. For example, the mean fidelity of the five experiments is only 0.677 and the standard deviation is 0.250 when quench time $T = 0.1$ ms. Yet the fidelity will tend to 1 and the standard deviation drops down synchronously once the time T increases to a certain value, e.g., when $T = 1$ ms, the mean value and standard deviation of the fidelities are 0.991 and 0.013, respectively. Figure 3(b) shows how the MAE of the three couplings, i.e., δJ_{ij} defined by Eq. (10), varies with respect to the time interval T. When the time T is short, the final states are close to the initial states, which makes the values in matrix M close to zero (as illustrated in Fig. 4 for different quench times T). As a result, the solution for $M\vec{x} = 0$ is more sensitive to the errors of the M matrix compared with the longer evolution time case. When T is large enough, the MAEs of the estimated parameters decrease to a certain level and start to oscillate due to the effect of other errors and fluctuations in the experiments. In this case, if one wants to further suppress the MAE in experiment, more pairs of initial and final states will work, as illustrated in Fig. 2. In addition, a too long time evolution will also produce nonignorable decoherence effects into the final results.

B. Analysis of the errors

The deviations between experimental couplings and theoretical results come from the imperfection of the M matrix. In general, the errors in our experiments can be divided into the following three types.

(i) Measurement error. Measurement error comes from the stochastic fluctuations of NMR spectra when we measure the expectation $\langle O_\alpha \rangle$. The standard deviation of each expectation is about $\Delta = 0.026$ according to the signal-to-noise ratio. As a result, the standard deviation of each element in the matrix M influenced by measurement error can be obtained from the error propagation formula

$$\Delta_m = \sqrt{2}\Delta \approx 0.037. \qquad (11)$$

Note that the value of every entry in the matrix $\mathbb{M}$ ranges from -2 to 2 in theory.

(ii) Decoherence. The quantum system inevitably interacts with the environment during the experimental process [42], thus introducing errors into the M matrix. Here we take the $T = 10$ ms case as an example and analyze the influence of decoherence. We simulate the effects of decoherence by introducing two noise channels into the ideal evolution [43].
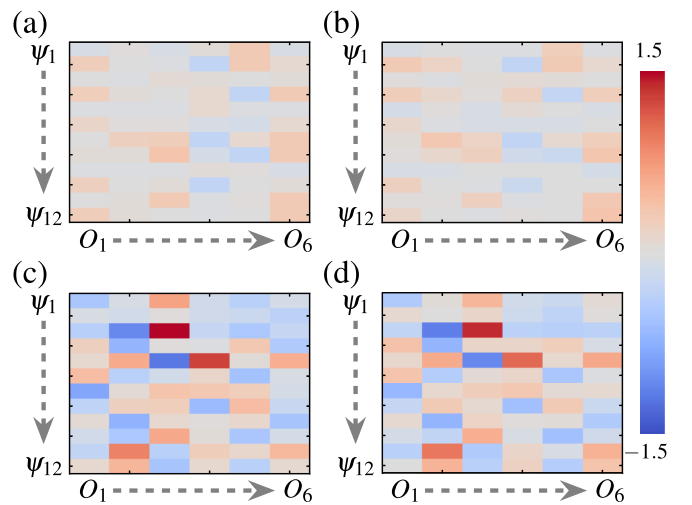

FIG. 4. (a) and (c) Theoretical $\mathbb{M}$ matrices and (b) and (d) corresponding experimental ones for the time intervals (a) and (b) $T = 0.5$ ms and (c) and (d) $T = 10$ ms. Here the number of quenches p is 12 and the color bar represents the values of M ($\mathbb{M}$) matrices. According to Eq. (16), the mean absolute errors Δ_{expt} are about 0.077 and 0.053 for $T = 10$ and 0.5 ms, respectively.

The first one is the phase damping channel $\mathcal{E}_{PD}$, which causes the off-diagonal elements of the density matrix to decay exponentially to zero with time. The second one is generalized amplitude damping $\mathcal{E}_{GAD}$, which describes the effect of dissipation to the environment. For short duration Δt, the influence of the phase damping channel on the system density matrix ρ is involved as $\rho \to \mathcal{E}_{PD}^3 \circ \mathcal{E}_{PD}^2 \circ \mathcal{E}_{PD}^1(\rho)$, where

$$\mathcal{E}_{PD}^j(\rho) = (1 - \xi_j)\rho + \xi_j \sigma_z^j \rho \sigma_z^j \tag{12}$$

and $\xi_j = \frac{1}{2}[1 - \exp(-\Delta t / T_2^j)]$. Here T_2^j is the transversal relaxation time of the jth qubit: $T_2^1 = 1.2$ s, $T_2^2 = 1.3$ s, and $T_2^3 = 1.1$ s [41]. Similarly, the generalized amplitude damping influence is characterized as $\rho \to \mathcal{E}_{GAD}^3 \circ \mathcal{E}_{GAD}^2 \circ \mathcal{E}_{GAD}^1(\rho)$ and it is calculated by

$$\mathcal{E}_{GAD}^j(\rho) = \sum_s E_s^j \rho E_s^{j\dagger}, \tag{13}$$

where

$$E_1^j = \sqrt{\xi_0}\begin{pmatrix} 1 & 0 \\ 0 & \sqrt{1-\eta^j} \end{pmatrix}, \quad E_2^j = \sqrt{1-\xi_0}\begin{pmatrix} 0 & 0 \\ \sqrt{\eta^j} & 0 \end{pmatrix},$$

$$E_3^j = \sqrt{1-\xi_0}\begin{pmatrix} \sqrt{1-\eta^j} & 0 \\ 0 & 1 \end{pmatrix}, \quad E_4^j = \sqrt{\xi_0}\begin{pmatrix} 0 & \sqrt{\eta^j} \\ 0 & 0 \end{pmatrix}, \tag{14}$$

with $\eta^j = 1 - \exp(-\Delta t / T_1^j)$, $\xi_0 \approx \frac{1}{2}$, and T_1^j the longitudinal relaxation time of the jth qubit: $T_1^1 = 2.8$ s, $T_1^2 = 3.1$ s, and $T_1^3 = 2.9$ s [41]. The M matrix influenced by decoherence can be determined numerically using the two noise channels above. Compared with the theoretical $\mathbb{M}$ matrix, the deviation Δ_d for each element in the matrix M is less than 0.005. It can be seen that the decoherence has little impact on the results since the experimental evolution time $T = 10$ ms is much shorter than the relaxation time.

(iii) Off-resonance error. During the experiments there exists thermal fluctuation of the NMR sample chemical shifts, which would introduce additional terms in Eq. (6), i.e., off-resonance effect [37]. Then the Hamiltonian of this physical system becomes

$$\mathbb{H}_{phys} = H_{phys} + \pi \sum_{k=1}^3 \omega_{off}^k \sigma_z^k, \tag{15}$$

where ω_{off}^k is the additional off-resonance shift (in hertz) for qubit k. In order to understand to what extent these shifts will affect the experimental results, we set $p = 12$ and $T = 10$ ms and numerically simulate the Hamiltonian (15) by randomly choosing $\omega_{off}^1 \in [-1, 1]$, $\omega_{off}^2 \in [-2, 2]$, and $\omega_{off}^3 \in [-2, 2]$. The result shows that the standard deviation Δ_{shift} for each element in the M matrix is less than 0.005 over 3000 simulations.

From the above analysis, we conclude that the three errors contribute to the total deviation Δ_{tot} about 0.04 for each element in the M matrix when $T = 10$ ms, and the measurement error plays a major role in our experiments. Figure 4(d) illustrates that the measured matrix M in the case of $T = 10$ ms,

$p = 12$, and the mean absolute error Δ_{expt} defined by

$$\Delta_{expt} = \frac{1}{p \cdot n} \sum_{i=1}^p \sum_{\alpha=1}^n |M_{i\alpha} - \mathbb{M}_{i\alpha}| \tag{16}$$

with respect to the theoretical matrix $\mathbb{M}$ [as shown in Fig. 4(c)] is 0.077, which is bigger than 0.04. This is because the imperfections of the initial state preparation also contribute to the errors in the experimental matrix M. However, there is reason to ignore its influence on the final reconstructed parameters because this method is suitable for any random initial state.

In addition, by adding random normal distribution errors with standard deviation Δ_{tot} to the perfect $\mathbb{M}$, the numerical results over 3000 simulations show that the reconstructed scaler coupling values are $J_{12} = 161.6 \pm 20.3$ Hz, $J_{23} = 48.1 \pm 17$ Hz, and $J_{13} = -196.3 \pm 36.9$ Hz when we take $p = 12$ and $T = 10$ ms. If we increase the number of initial states p to about 400, the simulated results would be $J_{12} = 160.7 \pm 3.0$ Hz, $J_{23} = 48.0 \pm 3.2$ Hz, and $J_{13} = -194.4 \pm 3.3$ Hz. We also compare this proposal with the one using the Fourier transform on temporal records of system observables [34]. Our NMR spectroscopy collects about 500 expectations $\langle \sigma_x \rangle$ and $\langle \sigma_y \rangle$ on three channels over a sampling duration of about 30 ms, and the resolution of scalar coupling constants obtained from the spectra are about 25 Hz. This indicates that the quantum quench method has advantages in both the number of measurements and experimental acquisition time.

IV. CONCLUSION

The quantum quench protocol can reconstruct the many-body Hamiltonian with local measurements of a few pairs of quantum states. In this work we implemented this method to determine the scalar couplings of a three-spin quantum system. By introducing the transverse rf field as reference, we successfully estimated the scalar couplings, which are close to the exact values. We also explored how the duration of the quench and the number of input states affect the quality of the estimation of this scheme. Future work may apply this scheme to estimate the unknown parameters of a Hamiltonian in more challenging systems like strong correlated systems, which usually have complex dipole-dipole interactions and short relaxation time. In short, our experiment proves the validity of the quantum quench protocol and provides a promising strategy to achieve many-body Hamiltonian tomography in different physical systems, such as ion traps [44] and superconducting circuits [45].

[1] I. M. Georgescu, S. Ashhab, and F. Nori, Quantum simulation, Rev. Mod. Phys. **86**, 153 (2014).

[2] A. Steane, Quantum computing, Rep. Prog. Phys. **61**, 117 (1998).

[3] V. Giovannetti, S. Lloyd, and L. Maccone, Quantum Metrology, Phys. Rev. Lett. **96**, 010401 (2006).

[4] J. H. Cole, Hamiltonian tomography: The quantum (system) measurement problem, New J. Phys. **17**, 101001 (2015).

[5] K. Vogel and H. Risken, Determination of quasiprobability distributions in terms of probability distributions for the rotated quadrature phase, Phys. Rev. A **40**, 2847 (1989).

[6] J. F. Poyatos, J. I. Cirac, and P. Zoller, Complete Characterization of a Quantum Process: The Two-Bit Quantum Gate, Phys. Rev. Lett. **78**, 390 (1997).

[7] A. I. Lvovsky and M. G. Raymer, Continuous-variable optical quantum-state tomography, Rev. Mod. Phys. **81**, 299 (2009).

[8] A. M. Childs, I. L. Chuang, and D. W. Leung, Realization of quantum process tomography in NMR, Phys. Rev. A **64**, 012314 (2001).

[9] T. van der Sar, Z. H. Wang, M. S. Blok, H. Bernien, T. H. Taminiau, D. M. Toyli, D. A. Lidar, D. D. Awschalom, R. Hanson, and V. V. Dobrovitski, Decoherence-protected quantum gates for a hybrid solid-state spin register, Nature (London) **484**, 82 (2012).

[10] G. D. Fuchs, A. L. Falk, V. V. Dobrovitski, and D. D. Awschalom, Spin Coherence During Optical Excitation of a Single Nitrogen-Vacancy Center in Diamond, Phys. Rev. Lett. **108**, 157602 (2012).

[11] B. Chen, J. Geng, F. Zhou, L. Song, H. Shen, and N. Xu, Quantum state tomography of a single electron spin in diamond with Wigner function reconstruction, Appl. Phys. Lett. **114**, 041102 (2019).

[12] Y. Nambu and K. Nakamura, Experimental Investigation of a Nonideal Two-Qubit Quantum-State Filter by Quantum Process Tomography, Phys. Rev. Lett. **94**, 010404 (2005).

[13] A. Shabani, R. L. Kosut, M. Mohseni, H. Rabitz, M. A. Broome, M. P. Almeida, A. Fedrizzi, and A. G. White, Efficient Measurement of Quantum Dynamics via Compressive Sensing, Phys. Rev. Lett. **106**, 100401 (2011).

[14] M. Riebe, K. Kim, P. Schindler, T. Monz, P. O. Schmidt, T. K. Körber, W. Hänsel, H. Häffner, C. F. Roos, and R. Blatt, Process Tomography of Ion Trap Quantum Gates, Phys. Rev. Lett. **97**, 220407 (2006).

[15] T. Monz, K. Kim, W. Hänsel, M. Riebe, A. S. Villar, P. Schindler, M. Chwalla, M. Hennrich, and R. Blatt, Realization of the Quantum Toffoli Gate with Trapped Ions, Phys. Rev. Lett. **102**, 040501 (2009).

[16] R. C. Bialczak, M. Ansmann, M. Hofheinz, E. Lucero, M. Neeley, A. D. O'Connell, D. Sank, H. Wang, J. Wenner, M. Steffen, A. N. Cleland, and J. M. Martinis, Quantum process tomography of a universal entangling gate implemented with Josephson phase qubits, Nat. Phys. **6**, 409 (2010).

[17] S. G. Schirmer, A. Kolli, and D. K. L. Oi, Experimental hamiltonian identification for controlled two-level systems, Phys. Rev. A **69**, 050306(R) (2004).

[18] J. H. Cole, S. G. Schirmer, A. D. Greentree, C. J. Wellard, D. K. L. Oi, and L. C. L. Hollenberg, Identifying an experimental two-state Hamiltonian to arbitrary accuracy, Phys. Rev. A **71**, 062312 (2005).

[19] S. J. Devitt, J. H. Cole, and L. C. L. Hollenberg, Scheme for direct measurement of a general two-qubit Hamiltonian, Phys. Rev. A **73**, 052317 (2006).

[20] E. H. Lapasar, K. Maruyama, D. Burgarth, T. Takui, Y. Kondo, and M. Nakahara, Estimation of coupling constants of a three-spin chain: A case study of Hamiltonian tomography with nuclear magnetic resonance, New J. Phys. **14**, 013043 (2012).

[21] C. Senko, J. Smith, P. Richerme, A. Lee, W. C. Campbell, and C. Monroe, Coherent imaging spectroscopy of a quantum many-body spin system, Science **345**, 430 (2014).

[22] A. Shabani, M. Mohseni, S. Lloyd, R. L. Kosut, and H. Rabitz, Estimation of many-body quantum Hamiltonians via compressive sensing, Phys. Rev. A **84**, 012107 (2011).

[23] L. Che, C. Wei, Y. Huang, D. Zhao, S. Xue, X. Nie, J. Li, D. Lu, and T. Xin, Learning quantum Hamiltonians from single-qubit measurements, arXiv:2012.12520.

[24] G. Torlai, C. J. Wood, A. Acharya, G. Carleo, J. Carrasquilla, and L. Aolita, Quantum process tomography with unsupervised learning and tensor networks, arXiv:2006.02424.

[25] D. Burgarth, K. Maruyama, and F. Nori, Coupling strength estimation for spin chains despite restricted access, Phys. Rev. A **79**, 020305(R) (2009).

[26] C. Di Franco, M. Paternostro, and M. S. Kim, Hamiltonian Tomography in an Access-Limited Setting without State Initialization, Phys. Rev. Lett. **102**, 187203 (2009).

[27] J. Zhang and M. Sarovar, Quantum Hamiltonian Identification from Measurement Time Traces, Phys. Rev. Lett. **113**, 080401 (2014).

[28] S.-Y. Hou, H. Li, and G.-L. Long, Experimental quantum Hamiltonian identification from measurement time traces, Sci. Bull. **62**, 863 (2017).

[29] J. R. Garrison and T. Grover, Does a Single Eigenstate Encode the Full Hamiltonian? Phys. Rev. X **8**, 021026 (2018).

[30] E. Chertkov and B. K. Clark, Computational Inverse Method for Constructing Spaces of Quantum Models from Wave Functions, Phys. Rev. X **8**, 031029 (2018).

[31] E. Bairey, I. Arad, and N. H. Lindner, Learning a Local Hamiltonian from Local Measurements, Phys. Rev. Lett. **122**, 020504 (2019).

[32] D. Burgarth and A. Ajoy, Evolution-Free Hamiltonian Parameter Estimation through Zeeman Markers, Phys. Rev. Lett. **119**, 030402 (2017).

[33] Z. Li, L. Zou, and T. H. Hsieh, Hamiltonian Tomography via Quantum Quench, Phys. Rev. Lett. **124**, 160502 (2020).

[34] J. Cavanagh, W. J. Fairbrother, A. G. Palmer III, and N. J. Skelton, *Protein NMR Spectroscopy: Principles and Practice* (Elsevier, Amsterdam, 1995).

[35] L. M. K. Vandersypen and I. L. Chuang, NMR techniques for quantum control and computation, Rev. Mod. Phys. **76**, 1037 (2005).

[36] G. Golub and C. Van Loan, *Matrix Computations* (Johns Hopkins University Press, Baltimore, 2013).

[37] M. H. Levitt, *Spin Dynamics: Basics of Nuclear Magnetic Resonance* (Wiley, New York, 2001).

[38] M. Ježek, J. Řeháček, and J. Fiurášek, Finding optimal strategies for minimum-error quantum-state discrimination, Phys. Rev. A **65**, 060301(R) (2002).

[39] X. Peng, X. Zhu, X. Fang, M. Feng, K. Gao, X. Yang, and M. Liu, Preparation of pseudo-pure states by line-selective pulses in nuclear magnetic resonance, Chem. Phys. Lett. **340**, 509 (2001).

[40] Y. Ji, J. Bian, X. Chen, J. Li, X. Nie, H. Zhou, and X. Peng, Experimental preparation of Greenberger-Horne-Zeilinger states in an Ising spin model by partially suppressing the nonadiabatic transitions, Phys. Rev. A **99**, 032323 (2019).

[41] X. Peng, S. Wu, J. Li, D. Suter, and J. Du, Observation of the Ground-State Geometric Phase in a Heisenberg *XY* Model, Phys. Rev. Lett. **105**, 240405 (2010).

[42] M. A. Nielsen and I. L. Chuang, *Quantum Computation and Quantum Information: 10th Anniversary Edition* (Cambridge University Press, Cambridge, 2010).

[43] L. M. Vandersypen, M. Steffen, G. Breyta, C. S. Yannoni, M. H. Sherwood, and I. L. Chuang, Experimental realization of Shor's quantum factoring algorithm using nuclear magnetic resonance, Nature (London) **414**, 883 (2001).

[44] J. Zhang, G. Pagano, P. W. Hess, A. Kyprianidis, P. B. Ecker, H. Kaplan, A. V. Gorshkov, Z. X. Gong, and C. Monroe, Observation of a many-body dynamical phase transition with a 53-qubit quantum simulator, Nature (London) **551**, 601 (2017).

[45] F. Arute, K. Arya, R. Babbush, D. Bacon, J. C. Bardin, R. Barends, R. Biswas *et al.*, Quantum supremacy using a programmable superconducting processor, Nature (London) **574**, 505 (2019).